ACS APPLIED MATERIALS & INTERFACES

Research Article

www.acsami.org

# $CH_3-\pi$ Interaction of Explosives with Cavity of a TPE Macrocycle: The Key Cause for Highly Selective Detection of TNT

Hai-Tao Feng, Jin-Hua Wang, and Yan-Song Zheng*

Key Laboratory for Large-Format Battery Materials and System, Ministry of Education, School of Chemistry and Chemical Engineering, Huazhong University of Science and Technology, Wuhan 430074, China

Supporting Information

**ABSTRACT:** The identification of explosives is critical for analyzing the background of terrorism activities and the origin of pollution aroused by the explosives, but it is a challenge to discriminate the explosives with a very similar structure. Herein we report a series of TPE-based macrocycles with an AIE effect for the 0.2−4 ppb level detection of TNT among a number of nitro-aromatic compounds through fluorescence quenching in natural water sources, whereas the contact mode approach using portable paper sensors exhibited a high sensitivity for the detection of TNT at $1.0 \times 10^{-13}$ M level. The reliability of the quantitative analysis has been confirmed by HPLC. Our findings demonstrate that the TPE-based macrocycles have great potential as excellent sensors for TNT. Moreover, it was found for the first time that the macrocycles could selectively recognize nitroaromatics explosives bearing methyl group through a $CH_3-\pi$ interactions, and even exhibit a sole selectivity for TNT among the very difficultly differentiating nitroaromatics including trinitrophenol and trinitrobenzene.

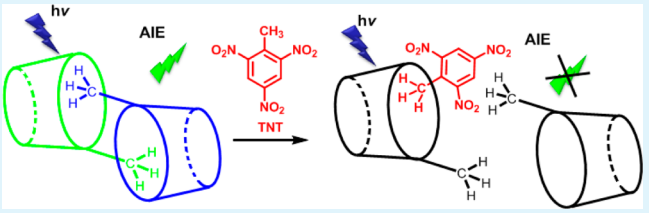


**KEYWORDS:** *tetraphenylethylene macrocycles, aggregation-induced emission, selective probe for TNT, $CH_3-\pi$ interaction, explosive sensor*

## INTRODUCTION

Because of the importance of counter-terrorism and environmental protection from widely used nitroaromatics, the detection of explosives has become an increasingly important and urgent issue.[1,2] To date, many suitably analytical methods have been used for the detection of explosives, such as gas chromatography, Raman spectroscopy, mass spectrometry, X-ray imaging, and so on.[3−7] Among these techniques, fluorescence sensing of explosives harnessing organic dyes has attracted the most attention because it is more simple, sensitive, and cost-effective.[8−11] Explosives are often multiple nitro organic compounds which are electron-deficient. They can arouse the fluorescence quenching of an electron-rich probe through a photoinduced electron transfer (PET) mechanism. Therefore, almost all the fluorescence probes are jointed with electron-rich functional groups which exhibit a very sensitive fluorescence response to the electron-deficient explosives.[8−11] However, the so prepared fluorescence probes lack selectivity although the determination of individual target from a similar class of explosives is critical for tracking the source of the explosives, seeking the origin of pollutants, and providing the detail-forceful forensic evidence. Under this situation, some research works on the selective detection of explosives have been done very recently.[12−16] For example, Moore and Zang et al.[12] reported a selectively diffusion-controlled detection of 2,4,6-trinitrotoluene (TNT) by fluorescence nanoporous fibers because the more electron-deficient TNT remained in the electron-rich nanopores while other nitroaromatic compounds (NACs) bearing less nitro groups were going out after the analyte vapor was removed. In contrast, Li et al.[13] reported a selective detection of nitrobenzene (NB) by a fluorescence microporous metal−organic framework (MOF) due to higher vapor pressure of NB than other NACs bearing more nitro groups. However, very rare work is reported on the selective detection among NACs bearing the same number of nitro groups such as trinitro NACs: TNT, 2,4,6-trinitrophenol (TNP), 1,3,5-trinitrobenzene (TNB), which are the most well-known and most widely used explosives. Moreover, the specific interactions between the electron-rich fluorescence probes and the electron-deficient explosives, whether $ArH-\pi$, $CH_3-\pi$, $\pi-\pi$, or others, are generally not known although it is helpful to the design of more excellent fluorescence probes for explosives.

Tetraphenylethylene (TPE) and its derivatives are a class of organic compounds that can exhibit a novel aggregation-induced emission (AIE) effect, and are extensively studied as chemo/biosensors and solid emitter.[17,18] For instance, they are tested as the fluorescence probes for TNT and TNP with high sensitivity, especially, with a superamplified quenching effect in sensing these two explosives.[19−24] But they generally exhibited no discrimination between TNT and TNP. To endow the TPE derivatives with better selectivity, very recently, macrocyclic compounds composed of TPE unit(s) started to be synthesized in our group.[25−29] The TPE macrocycles truly displayed a

Received: August 21, 2014
Accepted: October 16, 2014
Published: October 16, 2014

  

highly selectivity besides the high sensitivity. For example, a Schiff base TPE macrocycle[25] could differentiate the 2,4-dinitrophenol (DNP) from other NACs such as TNT, TNP, 2,4-dinitrotoluene (DNT), 1,3-dinitrobenzene (DNB), para-nitrotoluene (PNT), para-nitrophenol (PNP), and so on, because of the cavity size of the macrocycle that is suitable for including DNP. In the course of our continuous effort to develop excellent fluorescence probe for explosives, we report here that new electron-rich benzenedioxy TPE macrocycles are synthesized. It was found for the fist time that $CH_3-\pi$ interaction between TNT and the cavity of 1,2-benzenedioxy TPE macrocycle played a pivotal role on the exceptional selectivity for the detection of TNT among a series of NACs. Moreover, a completely new AIE mechanism of self-included dimer plus head−tail $\pi-\pi$ stacking of the TPE macrocycle in aggregate state endowed the macrocycle with a high quantum yield and a high sensitivity for the detection of TNT at $1.0 \times 10^{-13}$ M level.

## RESULTS AND DISCUSSION

The synthesis of benzenedioxy TPE macrocycles **5a**, **5b**, and **5c** is depicted in Scheme 1. The known AIE compound **1** was used as starting material, which was formylated by hexamethylenetetramine (HMTA) in trifluoroacetic acid (TFA) to give dialdehyde **2**. By a reduction of the dialdehyde **2** with sodium borohydride in ethanol/THF and the chloridization of the obtained dialcohol **3** by thionyl chloride in dichloromethane, the key intermediate dichloride **4** was obtained. The reaction of **4** with 1,2-benzenediol, 1,3-benzenediol, or 1,4-benzenediol in the presence of potassium carbonate gave the benzenedioxy TPE macrocycle **5a**, **5b**, and **5c**, respectively. All macrocycles were fully characterized by $^1$H NMR, $^{13}$C NMR, HRMS, and IR spectra.

**Scheme 1. Synthesis of Benzenedioxy TPE Macrocycle**

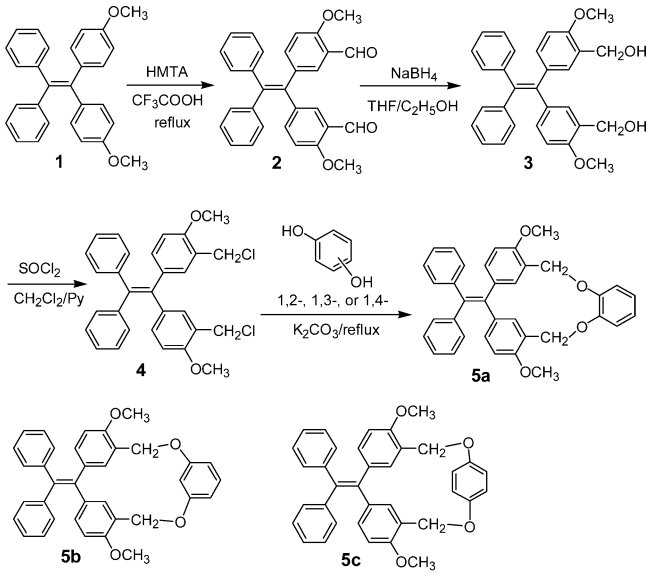


As expected, while the dilute solution of macrocycles in THF or chloroform had almost no fluorescence, their solids were blue green light emitting under irradiation of a 365 nm UV lamp. When the nonsolvent water was gradually added into the solution of the macrocycles in THF until a turbid appeared, the resultant suspension started to show fluorescence. After that, with the rising of water fraction in THF, the fluorescence intensity of the macrocycles increased (see Figure S13 in the Supporting Information). At 95% water, the fluorescence intensity of the resultant suspension was 801 fold larger than that of the solution in THF for **5a**, 166 fold for **5b**, and 38 fold for **5c**, indicating that all the benzenedioxy TPE macrocycles were AIE compounds. Moreover, a dynamic light scattering (DLS) diagram (see Figure S14 in the Supporting Information) showed that the suspension of TPE-cycles had a diameter from 100 to 250 nm in a mixed solvent of water/THF (95:5, v/v). The fluorescence quantum yields for the suspension of **5a**, **5b**, and **5c** in 95:5 $H_2O$/THF (volume ratio, the same below) were 48, 11, and 3.0%, companied with an emission maximum wavelength ($\lambda_{max}$) of 489, 478, and 466 nm, respectively. The gradually shortening of the emission $\lambda_{max}$ from **5a**, **5b**, to **5c** was in accordance with the successive decrease of the absorption $\lambda_{max}$ from **5a** (343 nm), **5b** (335 nm), to **5c** (325 nm) in THF (see Figure S15 in the Supporting Information).

The fluorescence response of the benzenedioxy TPE macrocycles **5a**, **5b** and **5c** in 95:5 $H_2O$/THF to the NACs including TNT, TNP, TNB, DNT, DNP, DNB, PNT, PNP, NB and phenol (P) (Scheme 2) was investigated. As shown in Figure 1, after 2 equiv. of different NACs were respectively added into the suspension of **5a** ($1.0 \times 10^{-6}$ M), only TNT and DNT significantly attenuated the fluorescence of the macrocycles (Figure 1A). The fluorescence intensity of **5a** at 489 nm was lessened to 30 and 412 from 767, which gave a fluorescence quenching efficiency (Figure 1B) of 96 and 46% for TNT and DNT, respectively. In contrast, by addition of TNB, only 18% quenching efficiency was obtained. Surprisingly, just like phenol, TNP aroused a little increase rather than decrease of the fluorescence of **5a**, giving a negative quenching efficiency of −7.4%. Other NACs including DNP, DNB, PNT, PNP, and NB displayed a quenching efficiency less than 8%. In the tests with **5b** and **5c**, the quenching efficiency also had the similar order to **5a**: TNT > DNT ≫ other NACs, but the quenching extent was less than that of **5a** (see Figure S16 in the Supporting Information).

**Scheme 2. Structure and the Abbreviation of NACs**

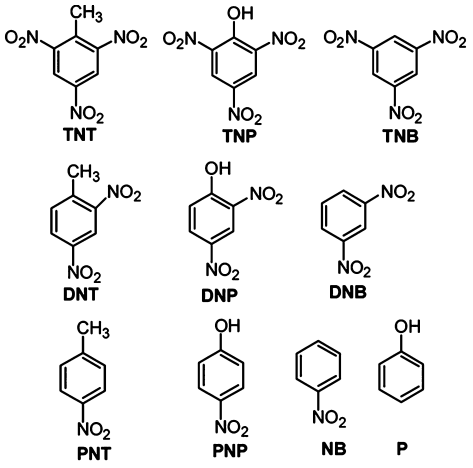


It has been reported that the fluorescence quenching of TPE derivatives by explosives usually had a superamplification quenching effect, that is, an exponential increase of $I_0/I$ with concentration of the explosives.[19−24] To know this, the

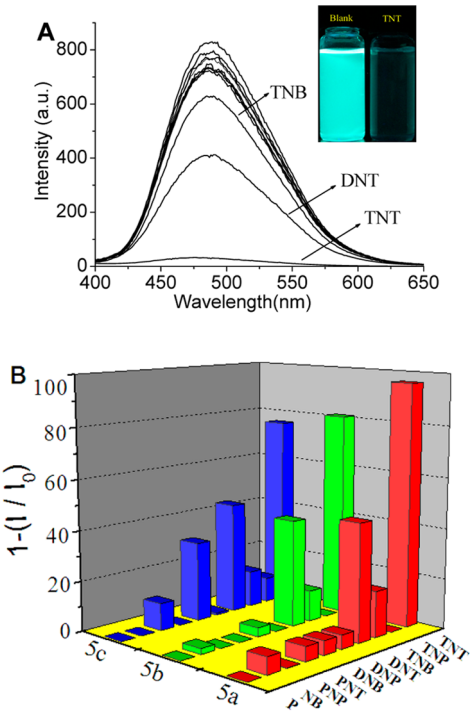


**Figure 1.** (A) Fluorescence spectra and (B) fluorescence quenching efficiency of **5a** in 95:5 $H_2O$/THF by addition of different NACs including phenol. The quenching efficiency = $(1 - I/I_0) \times 100\%$, I and $I_0$ denote the fluorescence intensity of **5a** with and without analyte, respectively. [**5a**] = $1.0 \times 10^{-6}$ M, [TNT] = [TNP] = [TNB] = [DNT] = [DNP] = [DNB] = [PNT] = [PNP] = [NB] = [P] = $2.0 \times 10^{-6}$ M, $\lambda_{ex}$ = 360 nm, ex/em slit widths = 5/5 nm.

fluorescence titrations of **5a** with TNT, TNB, DNT, and DNB were carried out. With gradual addition of TNT, TNB, DNT, or DNB, the fluorescence intensity of **5a** in 95:5 $H_2O$/THF decreased. But the fluorescence intensity had a rapid attenuation with concentration of TNT whereas it had only a slow decrease with concentration of TNB, DNT, or DNB. As a result, the intensity ratio $I_0/I$ had an exponential increase with TNT but a linear rise with TNB, DNT, or DNB (Figure 2).

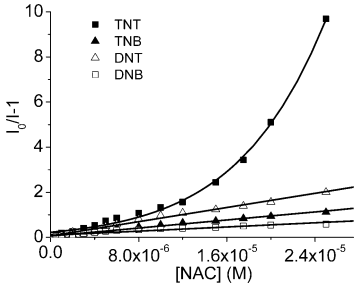


**Figure 2.** Fluorescence intensity ratio $(I_0/I - 1)$ of **5a** $(5.0 \times 10^{-6}$ M) changed with concentration of the selected NACs. in 95:5 $H_2O$/THF. $\lambda_{ex}$ = 360 nm, ex/em slit widths = 3/3 nm.

This indicated that only TNT had a superamplification quenching effect among the tested NACs. By using the exponential quenching equation $(I_0/I = Ae^{k[Q]}+B)$,[19] the quenching constants of **5a** with TNT was calculated to be $1.37 \times 10^5$ $M^{-1}$. According to the Stern−Volmer equation, the linear quenching constants of **5a** by TNB, DNT, and DNB was determined to be $4.5 \times 10^4$ $M^{-1}$, $7.9 \times 10^4$ $M^{-1}$, and $1.9 \times 10^4$ $M^{-1}$, respectively.

To determine the detection limits of TNT by **5a**, we measured the fluorescence change of $5.0 \times 10^{-7}$ M **5a** with different amounts of TNT in 95% water. As shown in Figure 3,

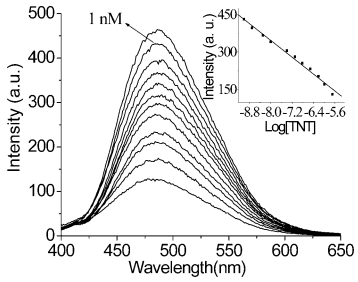


**Figure 3.** Change in fluorescence spectra of **5a** in 95:5 $H_2O$/THF with concentration of TNT. Inset, curve of fluorescence intensity of **5a** at 488 nm vs logarithm of concentration of TNT. $\lambda_{ex}$ = 360 nm, ex/em slit widths =5/5 nm. [**5a**] = $5.0 \times 10^{-7}$ M, [TNT] = 0, 0.010, 0.020, 0.050, 0.10, 0.40, 0.80, 1.0, 4.0, 8.0, 10, $20/10^{-7}$ M.

the fluorescence intensity of **5a** decreased with TNT. Even in the presence of $1.0 \times 10^{-9}$ M (0.22 μg/L, 0.22 ppb) TNT, the fluorescence intensity appeared a significant decrease. Moreover, the linear change in the fluorescence intensity versus the logarithm of concentration of TNT will be convenient for quantitative analysis of TNT in water. Considering the maximum permissible concentration of such hazardous substances in drinking water stipulated by the European Union that is 10 μg/L (10 ppb), **5a** could serve as a promising fluorescent probe for the detection of TNT. The other two macrocycles **5b** and **5c** also showed a sensitive response to TNT, and could be used to detect TNT at $10 \times 10^{-9}$ M and $20 \times 10^{-9}$ M levels (see Figure S17 in the Supporting Information).

To explore the practical applicability of the fluorescence macrocycles in natural environment, we tested a soil water sample. The soil water was prepared as the following. Soil was taken from farmland and fully mixed with deionized water. After leaving the mixture to stand for several hours, the supernatant was isolated by filtration to give the soil water. Then NACs and phenol was added into the soil water to be acted as the pollutants in soil. After the deionized water in the mixed solvent of 95:5 $H_2O$/THF was replaced by the soil water, the fluorescence quenching of **5a** by NACs and phenol was similar to that in the mixed solvent of deionized water/THF (Figure 4), demonstrating that other materials especially

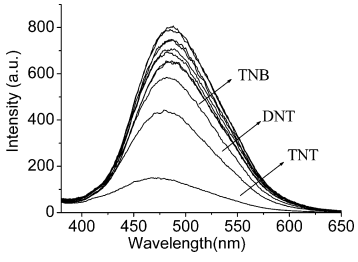


**Figure 4.** Fluorescence spectra of **5a** with addition of NACs and phenol in 95:5 soil water/THF. [**5a**] = $1.0 \times 10^{-6}$ M, [TNT] = [TNP] = [TNB] = [DNT] = [DNP] = [DNB] = [PNT] = [PNP] = [NB] = [P] = $2.0 \times 10^{-6}$ M, $\lambda_{ex}$ = 360 nm, ex/em slit widths =5/5 nm.


dx.doi.org/10.1021/am505636f | ACS Appl. Mater. Interfaces 2014, 6, 20067−20074

the metal ions in soil had not effect on the detection. In addition, the fluorescence intensity of **5a** decreased with the content of TNT in the soil water and displayed linear dependence between the intensity and the logarithm of TNT concentration. Therefore, the fluorescence probe **5a** could quantitatively detect TNT in soil, showing a high sensitivity almost the same as that in deionized water (Figure 5). The

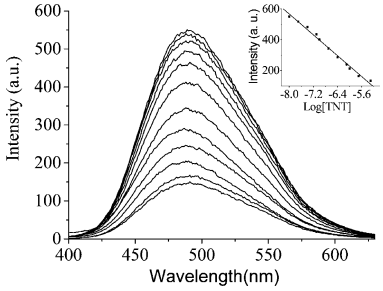


**Figure 5.** Change in the fluorescence spectra of **5a** with concentration of TNT in 95:5 soil water/THF. Inset, curve of fluorescence intensity of **5a** at 488 nm vs logarithm of concentration of TNT. $\lambda_{ex}$ = 360 nm, ex/em slit widths = 5/5 nm, [**5a**] = $5.0 \times 10^{-7}$ M, [TNT] = 0, 0.010, 0.020, 0.040, 0.080, 0.10, 0.20, 0.40, 0.80, 1.0, 2.0, $5.0/10^{-6}$ M.

reliability of quantitative analysis using **5a** was corroborated by HPLC analysis (see Figure S18 in the Supporting Information). A $1.0 \times 10^{-6}$ M solution of TNT in deionized water was used as a sample that needed to be measured. By drawing a HPLC standard curve, the sample was measured to be $1.08 \times 10^{-6}$ M, with an error of 8.0%. By making a fluorescence standard curve with **5a**, it was shown to be $1.05 \times 10^{-6}$ M, having an error of 5.0%. This confirmed that the quantitative analysis of TNT in the soil water using **5a** as fluorescence probe was reliable.

As an explosive sensor in the demand for homeland security and environmental safety, simplicity and rapidity are also highly desired besides sensitivity and selectivity. Taking this into account, a facile fluorescence test paper for the TNT analysis was developed. For this purpose, a filter paper strip (about 1.0 × 1.0 cm) was immersed into the solution of **5a** and then dried to get the TNT test paper. A 10 $\mu$L of TNT solution in 70:30 $H_2O/CH_3OH$ with different concentrations was spotted onto the center of the test paper to give a wet spot of approximately 0.5 $cm^2$. As soon as the test paper was air-dried, it was observed under a 365 nm UV lamp by the naked eye. It was found that the fluorescence intensity in the wetted area gradually decreased with increase of TNT concentration, and the minimum amount of TNT that could be detected by the naked eye was as low as $1.0 \times 10^{-13}$ M with a detection limit of approximately 0.45 pg $cm^{-2}$ (Figure 6). With **5b** and **5c**, the lowest concentration was $1.0 \times 10^{-11}$ M and $1.0 \times 10^{-10}$ M, respectively. The visual change in the fluorescence intensity on

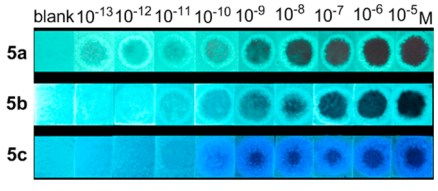


**Figure 6.** Photos of the fluorescence TNT test paper containing **5a**, **5b**, or **5c** before and after spotted with different concentrations of TNT under irradiation of a 365 nm UV lamp.

the test paper makes **5a** applicable to facile and instant detection of TNT onsite with very high sensitivity.

In most of related literatures for detection of explosives, TNT and TNP display nearly same quenching effect on the electron-rich fluorescence probes. In some cases, TNP was even used as a model sample for detection of TNT.[19−24] In our case, unlike TNT, TNP exhibited no any quenching effect. Compared TNB with TNT, TNB lacks the methyl group that is electron-donating and it will be more electron-deficient. Therefore, TNB will have stronger donor−acceptor interaction and stronger quenching effect on **5a** than TNT in theory. However, the fluorescence quenching efficiency of **5a** aroused by TNT is much larger than that by TNB. After checking the fluorescence quenching efficiency of **5a** by DNT, DNP, and DNB, it was also found that the quenching extent of **5a** by DNT was much bigger than that by DNP or DNB. Like TNP and TNB, DNP and DNB also lack the methyl group. Therefore, the methyl group should play a critical role on the fluorescence quenching of **5a**. Most probably, a $CH_3-\pi$ interaction was involved in the quenching process.

In order to confirm the $CH_3-\pi$ interaction, $^1$H NMR titrations of **5a** with TNT and $^1$H−$^1$H 2D NOESY NMR spectrum were carried out in $CDCl_3$ which could give better signals. When 2 mM **5a** in $CDCl_3$ was mixed with four molar equivalents of TNT, it could be found that the methoxyphenyl proton ($H_d$), methylene protons ($H_e$), and benzenedioxy protons ($H_f$, $H_g$) of **5a** exhibited an upfield shift of 0.0059, 0.0065, 0.0052, and 0.0072 ppm, respectively, whereas other protons had almost no chemical shift change (Figure 7).

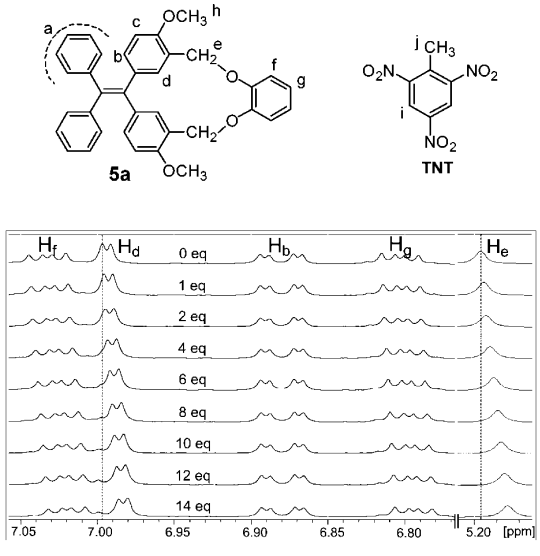


**Figure 7.** Structure of **5a** and TNT with their protons being marked by letters (upper) and change of $^1$H NMR spectra of **5a** with TNT in $CDCl_3$ (lower). [**5a**] = 2.0 mM. The number over the spectrum is the molar equivalents of TNT vs **5a**.

Meanwhile, the aromatic protons ($H_i$) and methyl protons ($H_j$) of TNT also showed an upfield shift of 0.0028 ppm. Although the change was not large, the protons' upfield shift of **5a** displayed an obviously gradual increase with TNT concentration. This ascertained the interaction between **5a** and TNT. Because it is strongly electron-deficient, TNT should make the protons of **5a** downfield shift rather than upfield shift according to the electron donor−acceptor interaction. The protons' upfield shift of **5a** hinted that these protons including $H_d$, $H_e$,

$H_f$, and $H_g$ were in the shielding area of the TNT aromatic ring. Only in the case of inclusion of TNT in the cavity of **5a** could the protons of two kinds of aromatic rings together with the methylene protons of **5a** enter into the shielding area of the TNT aromatic ring. Meanwhile, the protons of TNT also had an upfield shift under shielding of the aromatic rings of **5a** that formed the cavity.

The 2D NOESY spectrum of mixture of **5a** and TNT showed a distinct NOE signal between methyl proton ($H_j$) of TNT and methoxyphenyl proton ($H_d$) of **5a** (Figure 8 and

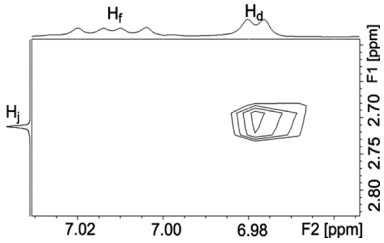


**Figure 8.** Partial 2D NOESY spectrum of the mixture of **5a** and TNT in $CDCl_3$. [**5a**] = 10 mM, [TNT] = 40 mM.

Figure S19 in the Supporting Information), indicating that the methyl group was pointing to the methoxyphenyl ring instead of the more electron-rich 1,2-benzenedioxy ring, probably because of the steric factor. No cross-peak between aromatic protons of TNT and protons of **5a** was found. Therefore, TNT was included into the cavity of **5a** from the side of its methyl group rather than the side of its aromatic proton. This confirmed the interaction of methyl group of TNT with aromatic ring of **5a**. For TNP, after mixed with **5a** in $CDCl_3$, the hydroxyl proton of it exhibited almost no any chemical shift change but this proton signal became wide and low, indicating an obvious OH-OAr hydrogen bond. However, there was no any NOE signal between hydroxyl proton or aromatic protons of it and protons of **5a**, demonstrating that TNP was probably not included in the cavity.

To have a clear insight into the AIE effect and the NAC-aroused fluorescence quenching of the benzenedioxy TPE macrocycles, single crystal of **5a** and **5c** suitable for crystal structure measurement was obtained by slow evaporation of their diluted solutions in $CHCl_3$ and methanol at room temperature.[30] As expected, the TPE unit in both **5a** and **5c** was twisted to be like a propeller (Figure 9A, B). From the crystal structure of **5a** (Figure 9A), the 1,2-benzenedioxy unit was protruded from the cycle rim and formed a more opening cavity together with one of the two methoxyphenyl rings. This resulted in less dihedral angle and more coplanarity between the methoxyphenyl ring and the double bond plane of **5a**, which brought longer absorption and emission $\lambda_{max}$. In contrast, in the crystal structure of **5c** (Figure 9B), the 1,4-benzenedioxy unit was located on the cycle rim and made the two methoxyphenyl rings keep away from the double bond plane, which resulted in shorter absorption and emission $\lambda_{max}$. With enlarging of the cycle, the increase of the dihedral angle and the decrease of coplanarity between the methoxyphenyl ring and the double bond plane led to a gradually shortened absorption and emission $\lambda_{max}$ from **5a**, **5b**, to **5c**.

By extracting the short contacts from the crystal structure of **5a**, a very novel phenomenon was revealed. Two molecules of **5a** can form a self-included dimer by $CH_3-\pi$ (2.783 Å) and ArH$-\pi$ (2.782 Å) interactions (Figure 9C). One methoxyl group of one molecule can insert into the cavity of another molecule by $CH_3-\pi$ interaction, whereas the methoxyl group of the later molecule can also insert into the cavity of the former molecule in the same way. Meanwhile, the ArH$-\pi$ interactions each other between the two molecules further consolidate the self-included dimer. It was worthy to note that the methyl group was also pointing to the methoxyphenyl ring rather than 1,2-benzenedioxy ring, which was in accordance with the result from 2D NMR measurement. The self-included dimer of **5a** demonstrated that the cavity of **5a** easily included methyl group by a $CH_3-\pi$ interaction, specifically, methoxyphenyl ring being easier to accept the methyl group. As long as the cavity of **5a** is inserted by the methyl of TNT, the fluorescence of **5a** will be quenched by a PET process and a high selectivity for TNT can be obtained.

More interesting, a lot of dimers can tightly link together through a $\pi-\pi$ stacking (3.324 Å) between unsubstituted phenyl rings of TPE units to form a 1D network (Figure 9D). These two phenyl rings in $\pi-\pi$ stacking have a dihedral angle of 0.00°, demonstrating that they are completely parallel. Therefore, this is a typical $\pi-\pi$ stacking interaction but in a head−tail way just like J-aggregation, which can give rise to fluorescence or fluorescence enhancement. As a result, aggregates of **5a** exhibited a fluorescence quantum yield much higher than that of **5b** and **5c**. The high quantum yield of the macrocycle can allow it to be used at a very low concentration, which can bring a high sensitivity. Due to the propeller structure of TPE unit, the phenyl rings are very difficult to form a $\pi-\pi$ stacking. To the best of our knowledge, this is the first example that TPE derivative can exist in a $\pi-\pi$ stacking in aggregate state.

Unexpectedly, $CH_3-\pi$ interaction (2.829 Å, 2.985 Å) was also observed in the crystal structure of **5c** (Figure 9E). Although the cycle of **5c** is larger than that of **5a**, the more twisted methoxyphenyl rings resulted in a small cavity that is not suitable for inclusion of a methyl group. Instead, the methyl group is included in the opening place between one unsubstituted phenyl ring and one methoxyphenyl ring of TPE unit. The molecules of **5c** can form a 1D network through $CH_3-\pi$ interactions each other but can not form a self-included dimer. The intermolecular $CH_3-\pi$ interaction of **5c** also provided it a high selectivity for TNT and DNT. In addition, no head−tail $\pi-\pi$ stacking was observed in the crystal structure of **5c**, therefore, the quantum yield of **5c** is not high. So much for that, it is very clear that the high quantum yield of **5a** (48%) compared with that of **5c** (3.0%) is aroused by the self-included dimer and head−tail $\pi-\pi$ stacking which were not existing in the crystal structure of **5c**. The formation of a self-included dimer by two TPE units could very efficiently limit the phenyl ring rotations of TPE units and enhanced the emission. TPE and its derivatives are the most studied AIE compounds,[17,18] but the mechanism underlying the AIE phenomenon is still bewildering and in dispute due to limited direct evidence.[31] This finding provides one new convincing evidence for AIE mechanism of TPE derivatives.

## CONCLUSION

In conclusion, three novel macrocycles were synthesized by bridging two phenyl rings of TPE with 1,2-benzenedioxy, 1,3-benzendioxy or 1,4-benzendioxy unit. It was found that the aggregate fluorescence of these TPE macrocycles could be quenched by TNT and DNT bearing a methyl group through a $CH_3-\pi$ interaction. Moreover, TNT exhibited a superamplified

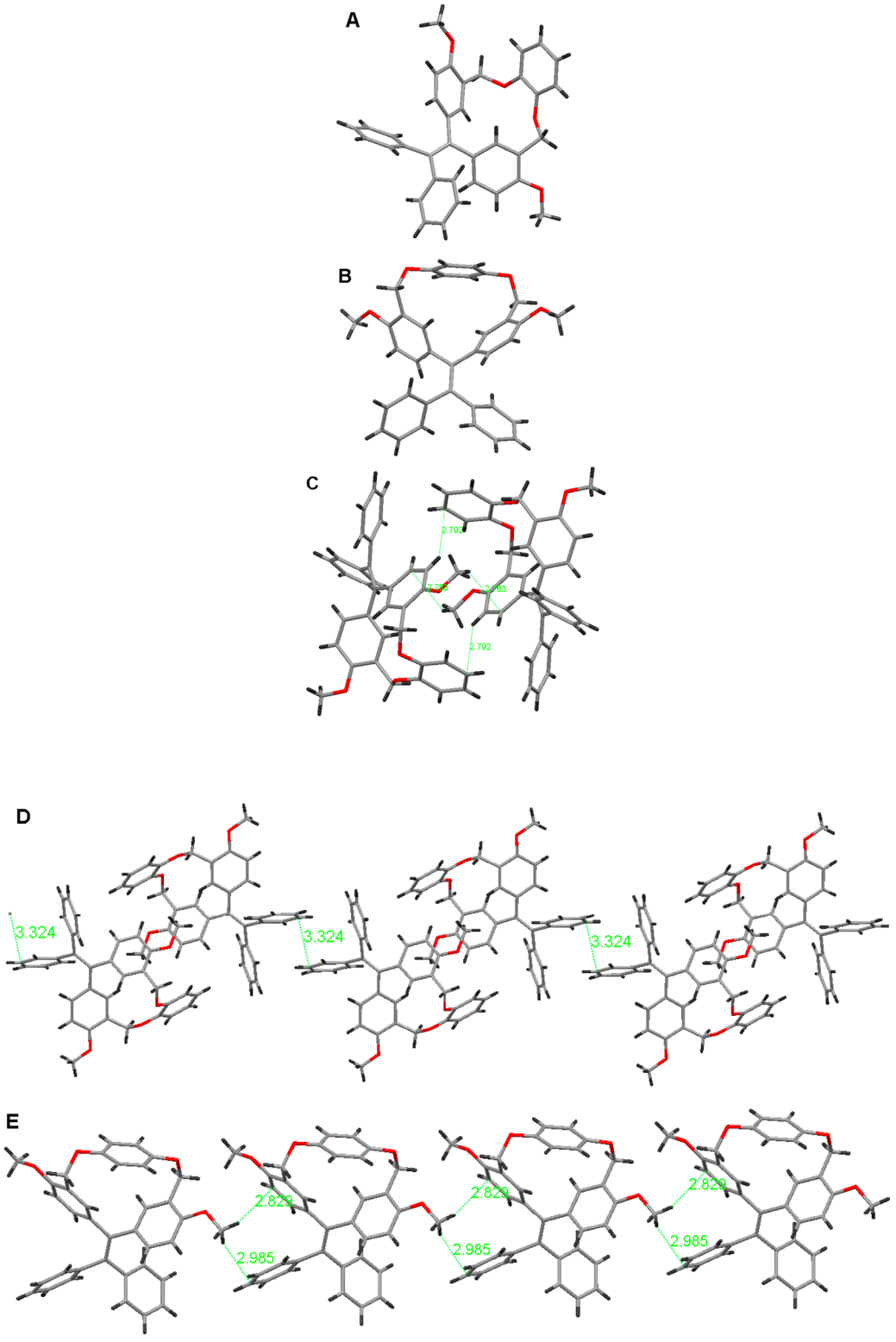


**Figure 9.** (A) Crystal structure of **5a**. (B) Crystal structure of **5c**. (C) Self-included dimer formed by $CH_3-\pi$ and ArH$-\pi$ interaction between two molecules of **5a**. (D) Head−tail $\pi-\pi$ stacking between the self-included dimers of **5a**. (E) 1D network formed by $CH_3-\pi$ interaction between molecules of **5c**.

quenching effect on the fluorescence of macrocycle **5a**, whereas DNT did not. Therefore, **5a** exhibited a sole recognition for TNT among the difficultly differentiating trinitroaromatics including TNP and TNB. In addition, the macrocycle **5a** could be prepared into TNT test paper, which could detect TNT at $1.0 \times 10^{-13}$ M level with a detection limit of 0.45 pg cm$^{-2}$. $^1$H NMR titration, 2D NOESY spectrum and crystal structure of **5a** and **5c** confirmed the $CH_3-\pi$ interaction. Moreover, macrocycle **5a** could form a self-included dimer and heat-tail $\pi-\pi$ stacking in aggregate state, which brought **5a** a high quantum yield and a very high sensitivity for detection of TNT. This finding not only has exceptional novelty but also provides

a completely new idea to design excellent TNT fluorescence probe.

## EXPERIMENTAL SECTION

**Materials.** All reagents and solvents were chemical pure (CP) grade or analytical reagent (AR) grade and were used as received unless otherwise indicated.

**Caution.** PA, TNT, and other NACs used in the present study are highly explosive and should be handled only in small quantities.

**Measurements.** $^1$H NMR and $^{13}$C NMR spectra were measured on a Bruker AV 400 spectrometer at 298 K in $CDCl_3$. Infrared spectra were recorded on BRUKER EQUINAX55 spectrometer. Absorption spectra were recorded on a Hewlett-Packard 8453 UV−vis spectrophotometer. Mass spectrum was measured on an IonSpec 4.7 T FTMS instrument. Fluorescent emission spectra were collected on a Shimadzu RF-5301 fluorophotometer at 298 K. The fluorescence spectra for AIE effect were measured after water was added and let the mixture stand for 4 h at 298 K. For measuring change of fluorescence intensity with explosives, all mixtures of **5a**, **5b**, **5c** and explosives were left standing for 8 h at 298 K before their fluorescence spectra were measured. HPLC analysis of TNT concentration was carried out on a Agilent 1100 HPLC instrument under the following conditions: 4.6 × 250 mm Agilent HC-$C_{18}$ column at 35 °C, detection wavelength 225 nm, mobile phase: 50:50 mathanol/water (V/V) with a flow velocity of 0.5 mL/min. The soil which was taken from farmland was mixed with tap water; the weight ratio of water/soil was 10:1. After the mixture was left standing for several hours, the supernatant was isolated by filtration.

*Synthesis of 1,2-Benzenedioxy TPE Macrocycle* ***5a***. To a solution of **4** (0.20 g, 0.409 mmol) in anhydrous acetonitrile (15 mL) was added potassium carbonate (0.226 g, 1.624 mmol). After the reaction mixture was stirred for 30 min at room temperature, 1,2-dihydroxybenzene (0.054 g, 0.4904 mmol) was added and the mixture was refluxed for 24 h. Acetonitrile was removed under vacuum and $CH_2Cl_2$ (30 mL) was added. The mixture was washed twice with water and dried over anhydrous sodium sulfate. The solvent was evaporated and the residue was purified by flash column chromatography to afford **5a** as a pale yellow solid (0.04 g, 19%). Mp = 241.2−241.9 °C. $^1$H NMR ($CDCl_3$, 400 MHz) $\delta$ = 3.76 (s, 6H), 5.19 (s, 4H), 6.42 (d, $J$ = 8.6 Hz, 2H), 6.80 (dd, $J$ = 3.6, 6.0 Hz, 2H), 6.86 (d, $J$ = 2.1 Hz, 1H), 6.89 (d, $J$ = 2.1 Hz, 1H), 6.99 (d, $J$ = 2.0 Hz, 2H), 7.03 (dd, $J$ = 3.6, 5.9 Hz, 2H), 7.14 (m, 10H) ppm. $^{13}$C NMR ($CDCl_3$, 100 MHz) $\delta$ = 55.40, 65.09, 109.30, 116.15, 121.15, 124.81, 126.41, 127.96, 131.53, 134.22, 136.00, 136.22, 137.56, 139.04, 145.05, 149.58, 155.77 ppm. IR (film): $\nu_{max}$ = 3051.6, 3026.5, 2925.1, 2835.7, 1595.2, 1500.8, 1462.4, 1444.6, 1363.2, 1252.5, 1187.5, 1111.7, 1026.6, 988.5, 819.0, 744.9, 699.6 cm$^{-1}$. HRMS (ESI$^+$): Calcd for $C_{36}H_{31}O_4$ 527.2222 [M + H]$^+$, Found 527.2225.

*Synthesis of 1,3-Benzenedioxy TPE Macrocycle* ***5b***. the procedure was similar to that of **5a**. The title compound was synthesized from **4** and 1,3-dihydroxybenzene and was obtained as a white solid (yield, 65%). Mp = 217.2−218.1 °C. $^1$H NMR ($CDCl_3$, 400 MHz) $\delta$ = 3.79 (s, 6H), 5.04 (s, 4H), 5.98 (s, 1H), 6.46 (d, $J$ = 8.5 Hz, 2H), 6.57 (d, $J$ = 2.0 Hz, 1H), 6.59 (d, $J$ = 2.0 Hz, 1H), 6.63 (d, $J$ = 1.9 Hz, 2H), 6.88 (d, $J$ = 2.0 Hz, 1H), 6.90 (d, $J$ = 2.0 Hz, 1H), 7.00−7.06 (m, 5H), 7.09−7.19(m, 6H) ppm. $^{13}$C NMR ($CDCl_3$, 100 MHz) $\delta$ = 55.49, 69.12, 109.50, 112.62, 113.72, 124.05, 126.24, 127.80, 129.48, 131.49, 133.57, 134.43, 135.45, 138.63, 139.43, 144.61, 156.45, 158.84 ppm. IR (film): $\nu_{max}$ = 3066.2, 3019.0, 2911.0, 2835.2, 1594.3, 1501.1, 1441.8, 1328.9, 1251.7, 1125.8, 1028.8, 966.7, 694.8 cm$^{-1}$. HRMS (ESI$^+$): Calcd for $C_{36}H_{31}O_4$ 527.2222 [M + H]$^+$, Found 527.2222.

*Synthesis of 1,4-Benzenedioxy TPE Macrocycle* ***5c***. the procedure was similar to that of **5a**. The title compound was synthesized from **4** and 1,4-dihydroxybenzene and was obtained as a white solid (yield, 52%). Mp = 233.9−234.6 °C. $^1$H NMR ($CDCl_3$, 400 MHz) $\delta$ = 3.84 (s, 6H), 4.96 (s, 4H), 6.11 (d, $J$ = 2.0 Hz, 2H), 6.48 (d, $J$ = 8.5 Hz, 2H), 6.52 (s, 4H), 6.80 (d, $J$ = 2.1 Hz, 1H), 6.82 (d, $J$ = 2.2 Hz, 1H), 6.88−6.90 (m, 4H), 7.04−7.06 (m, 6H) ppm. $^{13}$C NMR ($CDCl_3$, 100 MHz) $\delta$ = 55.60, 71.92, 109.30, 122.54, 123.69, 126.04, 127.63, 131.32, 133.62, 134.90, 135.42, 139.47, 139.62, 144.19, 153.15, 157.10 ppm. IR (film): $\nu_{max}$ = 3051.4, 3007.9, 2919.7, 2852.2, 1603.5, 1501.4, 1443.8, 1363.4, 1253.5, 1186.1, 1028.4, 961.3, 823.7, 700.4 cm$^{-1}$. HRMS (ESI$^+$): calcd for $C_{36}H_{31}O_4$, 527.2222 [M + H]$^+$; found, 527.2225.

## ASSOCIATED CONTENT

### Supporting Information

Experimental detail and characterization data including $^1$H NMR, $^{13}$C NMR, HRMS spectra, and HPLC spectrum. This material is available free of charge via the Internet at http://pubs.acs.org.

## AUTHOR INFORMATION

### Corresponding Author

*E-mail: zyansong@hotmail.com.

### Author Contributions

The manuscript was written through contributions of all authors./All authors have given approval to the final version of the manuscript.

### Notes

The authors declare no competing financial interest.

## ACKNOWLEDGMENTS

The authors thank National Natural Science Foundation of China (21072067) for financial support and thank the Analytical and Testing Centre at Huazhong University of Science and Technology for measurement.

## REFERENCES

(1) Steinfeld, J. I.; Wormhoudt, J. Explosives Detection: A Challenge for Physical Chemistry. *Annu. Rev. Phys. Chem.* **1998**, *49*, 203−232.

(2) Afzala, A.; Iqbala, N.; Mujahida, A.; Schirhagl, R. Advanced Vapor Recognition Materials for Selective and Fast Responsive Surface Acoustic Wave Sensors: A Review. *Anal. Chim. Acta* **2013**, *787*, 36−49.

(3) Pablos, J. L.; Garcia, J. M. Water-Soluble Polymers, Solid Polymer Membranes, and Coated Fibres as Smart Sensory Materials for the Naked Eye Detection and Quantification of TNT in Aqueous Media. *Chem. Commun.* **2014**, *50*, 2484−2487.

(4) Cooks, R. G.; Ouyang, Z.; Takats, Z.; Wiseman, J. M. Ambient Mass Spectrometry. *Science* **2006**, *311*, 1566−1570.

(5) Caygill, J. S.; Davis, F.; Higson, S. P. J. Current Trends in Explosive Detection Techniques. *Talanta* **2012**, *88*, 14−29.

(6) Kuligowskia, J.; Quintása, G.; de la Guardiaa, M.; Lendl, B. Analytical Potential of Mid-Infrared Detection in Capillary Electrophoresis and Liquid Chromatography: A Review. *Anal. Chim. Acta* **2010**, *679*, 31−42.

(7) Gottfried, J. L.; Lucia, F. C. D., Jr; Munson, C. A.; Miziolek, A. W. Laser-Induced Breakdown Spectroscopy for Detection of Explosives Residues: A Review of Recent Advances, Challenges, and Future Prospects. *Anal. Bioanal. Chem.* **2009**, *395*, 283−300.

(8) Salinas, Y.; Martınez-Manez, R.; Marcos, M. D.; Sancenón, F.; Costero, A. M.; Parra, M.; Gil, S. Optical Chemosensors and Reagents to Detect Explosives. *Chem. Soc. Rev.* **2012**, *41*, 1261−1296.

(9) Germain, M. E.; Knapp, M. J. Optical Explosives Detection: from Color Changes to Fluorescence Turn-on. *Chem. Soc. Rev.* **2009**, *38*, 2543−2555.

(10) Kartha, K. K.; Babu, S. S.; Srinivasan, S.; Ajayaghosh, A. Attogram Sensing of Trinitrotoluene with a Self-Assembled Molecular Gelator. *J. Am. Chem. Soc.* **2012**, *134*, 4834−4841.

(11) Gopalakrishnan, D.; Dichtel, W. R. Direct Detection of RDX Vapor Using a Conjugated Polymer Network. *J. Am. Chem. Soc.* **2013**, *135*, 8357−8362.

(12) Che, Y.; Gross, D.; Moore, J. S.; Zang, L. Diffusion-Controlled Detection of Trinitrotoluene: Interior Nanoporous Structure and Low

Highest Occupied Molecular Orbital Level of Building Blocks Enhance Selectivity and Sensitivity. *J. Am. Chem. Soc.* **2012**, *134*, 4978−4982.
(13) Pramanik, S.; Zheng, C.; Zhang, X.; Emge, T. J.; Li, J. New Microporous Metal-Organic Framework Demonstrating Unique Selectivity for Detection of High Explosives and Aromatic Compounds. *J. Am. Chem. Soc.* **2011**, *133*, 4153−4155.
(14) Salinas, Y.; Climent, E.; Martínez-Máñez, R.; Sancenón, F.; Marcos, M. D.; Soto, J.; Costero, A. M.; Gil, S.; Parraad, M.; de Diego, A. P. Highly Selective and Sensitive Chromo-Fluorogenic Detection of the Tetryl Explosive Using Functional Silica Nanoparticles. *Chem. Commun.* **2011**, *47*, 11885−11887.
(15) Ma, Y.; Huang, S.; Deng, M.; Wang, L. White Upconversion Luminescence Nanocrystals for the Simultaneous and Selective Detection of 2,4,6-Trinitrotoluene and 2,4,6-Trinitrophenol. *ACS Appl. Mater. Interfaces* **2014**, *6*, 7790−7796.
(16) Xu, B.; Wu, X.; Li, H.; Tong, H.; Wang, L. Selective Detection of TNT and Picric Acid by Conjugated Polymer Film Sensors with Donor−acceptor architecture. *Macromolecules* **2011**, *44*, 5089−5092.
(17) Hong, Y.; Lam, J. W. Y.; Tang, B. Z. Aggregation-Induced Emission. *Chem. Soc. Rev.* **2011**, *40*, 5361−5388.
(18) Wang, M.; Zhang, G.; Zhu, D.; Tang, B. Z. Fluorescent Bio/Chemosensors Based on Silole and Tetraphenylethene Luminogens with Aggregation-Induced Emission Feature. *J. Mater. Chem.* **2010**, *20*, 1858−1867.
(19) Liu, J.-Z.; Zhong, Y.-C.; Lu, P.; Hong, Y.-N.; Lam, J. W. Y.; Faisal, M.; Yu, Y.; Wong, K. S.; Tang, B.-Z. A Superamplification Effect in the Detection of Explosives by a Fluorescent Hyperbranched Poly (silylenephenylene) with Aggregation-Enhanced Emission Characteristics. *Polym. Chem.* **2010**, *1*, 426−429.
(20) Yuan, W. Z.; Zhao, H.; Shen, X. Y.; Mahtab, F.; Lam, J. W. Y.; J. Sun, Z.; Tang, B. Z. Luminogenic Polyacetylenes and Conjugated polyelectrolytes: synthesis, hybridization with carbon nanotubes, Aggregation-Induced Emission, Superamplification in Emission Quenching by Explosives, and Fluorescent Assay for Protein Quantitation. *Macromolecules* **2009**, *42*, 9400−9411.
(21) Hu, R.; Maldonado, J. L.; Rodriguez, M.; Deng, C.; Jim, C. K. W.; Lam, J. W. Y.; Yuen, M. M. F.; Ramos-Ortiz, G.; Tang, B. Z. Luminogenic Materials Constructed from Tetraphenylethene Building Blocks: Synthesis, Aggregation-Induced Emission, Two-Photon Absorption, Light Refraction, and Explosive Detection. *J. Mater. Chem.* **2012**, *22*, 232−240.
(22) Qin, A.; Lam, J. W. Y.; Tang, L.; Jim, C. K. W.; Zhao, H.; Sun, J.; Tang, B. Z. Polytriazoles with Aggregation-Induced Emission Characteristics: Synthesis by Click Polymerization and Application as Explosive Chemosensors. *Macromolecules* **2009**, *42*, 1421−1424.
(23) Liu, J.; Zhong, Y.; Lam, J. W. Y.; Lu, P.; Hong, Y.; Yu, Y.; Yue, Y.; Faisal, M.; Sung, H. H. Y.; Williams, I. D.; Wong, K. S.; Tang, B. Z. Hyperbranched Conjugated Polysiloles: Synthesis, Structure, Aggregation-Enhanced Emission, Multicolor Fluorescent Photopatterning, and Superamplified Detection of Explosives. *Macromolecules* **2010**, *43*, 4921−4936.
(24) Li, H.; Wu, H.; Zhao, E.; Li, J.; Sun, J. Z.; Qin, A.; Tang, B. Z. Hyperbranched Poly(aroxycarbonyltriazole)s: Metal-Free Click Polymerization, Light Refraction, Aggregation-Induced Emission, Explosive Detection, and Fluorescent Patterning. *Macromolecules* **2013**, *46*, 3907−3910.
(25) Feng, H.-T.; Zheng, Y.-S. Highly Sensitive and Selective Detection of Nitrophenolic Explosives by Using Nanospheres of a Tetraphenylethylene Macrocycle Displaying Aggregation-Induced Emission. *Chem.—Eur. J.* **2014**, *20*, 195−201.
(26) Feng, H.-T.; Song, S.; Chen, Y.-C.; Shen, C. H.; Zheng, Y.-S. Self-Assembled Tetraphenylethylene Macrocycle Nanofibrous Materials for the Visual Detection of Copper (II) in Water. *J. Mater. Chem. C* **2014**, *2*, 2353−2359.
(27) Wang, J.-H.; Feng, H.-T.; Luo, J.; Zheng, Y.-S. Monomer Emission and Aggregate Emission of an Imidazolium Macrocycle Based on Bridged Tetraphenylethylene and Their Quenching by C60. *J. Org. Chem.* **2014**, *79*, 5746−5751.
(28) Song, S.; Zheng, Y.-S. Monomer Emission and Aggregate Emission of TPE Derivatives in the Presence of γ-Cyclodextrin. *Org. Lett.* **2013**, *15*, 820−823.
(29) Zhang, C.; Wang, Z.; Song, S.; Meng, X.; Zheng, Y.-S.; Yang, X.-L.; Xu, H.-B. Tetraphenylethylene-Based Expanded Oxacalixarene: Synthesis, Structure, and Its Supramolecular Grid Assemblies Directed by Guests in the Solid State. *J. Org. Chem.* **2014**, *79*, 2729−2732.
(30) The crystallographic data have been deposited in the Cambridge Structural Database as CCDC 1008373 for **5a** and CCDC 1008374 for **5c**.
(31) Zhao, Z.; He, B.; Nie, H.; Chen, B.; Lu, P.; Qin, A.; Tang, B. Z. Stereoselective Synthesis of Folded Luminogens with Arene−Arene Stacking Interactions and Aggregation-Enhanced Emission. *Chem. Commun.* **2014**, *50*, 1131−1133.